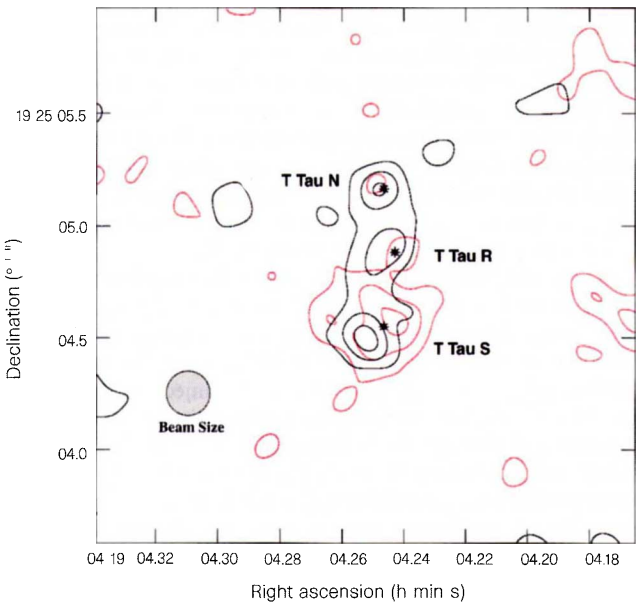

Figure 3 MERLIN contour map of the 6-cm radio emission in the T Tau region. Right- and left-hand circularly polarized components are shown in red and black respectively. Contour levels are in each case 0.4, 0.8 and 1.2 mJy, right ascension and declination are in B1950 coordinates. Note the spatially resolved separation of the emission from T Tau S into two lobes of opposite helicity and the net left-hand circular polarization of T Tau N. Thus the 'flow' and 'counterflow' from T Tau S are both circularly polarized but in opposite senses. The source positions (see Table 1) are shown as asterisks.

velocities) have been determined through imaging and spectroscopic studies[3], magnetic field strengths have remained elusive. Polarization studies at a range of radio frequencies could provide us with the necessary diagnostic tool. Moreover, given that the radio emission from a number of other outflows is suspected of being non-thermal[25], such studies could in principle allow us to test currently favoured models of the magnetic collimation of outflows from young stars. We intend to continue monitoring T Tau S outflow at radio wavelengths to see how this outflow evolves with time. It should be possible not only to test the shock hypothesis but also, through proper-motion studies, to link unambiguously the radio outflow activity with what was probably a major accretion event in the life of a newborn star. □

Received 9 October; accepted 31 December 1996.

1. Bertout, C. *Annu. Rev. Astron. Astrophys.* **27,** 351–395 (1989).
2. Beckwith, S. V. W. & Sargent, A. I. *Nature* **383,** 139–144 (1996).
3. Edwards, S., Ray, T. P. & Mundt, R. in *Protostars and Planets III* (eds Levy, E. & Lunine, J.) 567–602 (Univ. Arizona Press, Tucson, 1993).
4. Königl, A. & Ruden, S. P. in *Protostars and Planets III* (eds Levy, E. & Lunine, J.) 641–687 (Univ. Arizona Press, Tucson, 1993).
5. Dyck, H. M., Simon, T. & Zuckerman, B. *Astrophys. J.* **255,** L103–L106 (1982).
6. Solf, J., Böhm, K. H. & Raga, A. C. *Astrophys. J.* **334,** 229–251 (1988).
7. Böhm, K. H. & Solf, J. *Astrophys. J.* **430,** 277–290 (1994).
8. Ghez, A. M. *et al. Astron. J.* **102,** 2066–2072 (1991).
9. Ghez, A. M., Weinberger, A. J., Neugebauer, G., Matthews, K. & McCarthy, Jr. D. W. *Astron. J.* **110,** 753–765 (1995).
10. Schwartz, P. R., Simon, T., Zuckerman, B. & Howell, R. R. *Astrophys. J.* **280,** L23–L26 (1984).
11. Skinner, S. L. & Brown, A. *Astron. J.* **107,** 1461–1468 (1994).
12. Philips, R. B., Lonsdale, C. J. & Feigelson, E. D. *Astrophys. J.* **403,** L43–L46 (1993).
13. Nisenson, P., Stachnik, R. V., Karovska, M. & Noyes, R. *Astrophys. J.* **297,** L17–L20 (1985).
14. Maihara, T. & Kataza, H. *Astron. Astrophys.* **249,** 392–396 (1991).
15. Gorham, P. W. *et al. Astron. J.* **103,** 953–959 (1992).
16. Schwartz, P. R., Simon, T. & Campbell, R. *Astrophys. J.* **303,** 233–238 (1986).
17. *Carlsberg Meridian Catalogue No. 4* (Copenhagen Univ. Observatory, Royal Greenwich Observatory, Real Instituto y Observatorio de la Armada en San Fernando, 1989).
18. Kenyon, S. J., Dobrzycka, D. & Hartmann, L. *Astron. J.* **108,** 1872–1880 (1994).
19. Skinner, S. L. *Astrophys. J.* **408,** 660–667 (1993).
20. Dulk, G. A. *Annu. Rev. Astron. Astrophys.* **23,** 169–224 (1985).
21. Guenther, E. W. & Emerson, J. P. *Astron. Astrophys.* **309,** 777–780 (1996).
22. van Langvelde, H. J., van Dishoeck, E. F., van der Werf, P. P. & Blake, G. A. *Astron. Astrophys.* **287,** L25–L28 (1994).
23. Roberto, M. *et al. Astron. Astrophys.* **296,** 431–438 (1995).
24. Herbig, G. H. in *Low Mass Star Formation and Pre-Main Sequence Objects* (ed. Reipurth, B.) 233–246 (ESO Conf. and Workshop Proc. no. 33, ESO, Munich, 1989).
25. Curiel, S., Rodríguez, L. F., Moran, J. M. & Canto, J. *Astrophys. J.* **415,** 191–203 (1993).

Acknowledgements. We thank L. Morrison for his assistance with the Carlsberg Automatic Meridian Circle data; L. Drury, T. Herbst and J. Stone for comments on the manuscript; and T. Herbst and K. Hodapp for allowing us to reproduce their images. A.B. was supported by NASA. MERLIN is a national facility operated by the University of Manchester on behalf of the UK Particle Physics and Astronomy Research Council (PPARC).

Correspondence should be addressed to T.P.R. (e-mail: tpr@cp.dias.ie).

Phase measurement in a quantum dot via a double-slit interference experiment

R. Schuster, E. Buks, M. Heiblum, D. Mahalu, V. Umansky & Hadas Shtrikman

Braun Center for Submicron Research, Department of Condensed Matter Physics, Weizmann Institute of Science, Rehovot 76100, Israel

The transport properties of electronic devices are usually characterized on the basis of conductance measurements. Such measurements are adequate for devices in which transport occurs incoherently, but for very small devices—such as quantum dots[1,2]—the wave nature of the electrons plays an important role[3]. Because the phase of an electron's wavefunction changes as it passes through such a device, phase measurements are required to characterize the transport properties fully. Here we report the results of a double-slit interference experiment which permits the measurement of the phase-shift of an electron traversing a quantum dot. This is accomplished by inserting the quantum dot into one arm of an interferometer, thereby introducing a measurable phase shift between the arms. We find that the phase evolution within a resonance of the quantum dot can be accounted for qualitatively by a model that ignores the interactions between the electrons within the dot. Although these electrons must interact strongly, such interactions apparently have no observable effect on the phase. On the other hand, we also find that the phase behaviour is identical for all resonances, and that there is a sharp jump of the phase between successive resonance peaks. Adequate explanation of these features may require a model that includes interactions between electrons.

In a previous interference experiment[3], which exploited an Aharonov–Bohm (AB) ring (see ref. 4 for review) and a quantum dot (QD) imbedded in it, the conductance was shown to depend not only on the magnitude of the transmission through the QD, but also on the phase acquired by electrons traversing the QD. The observed oscillatory behaviour of the conductance, G, which was periodic with the flux quantum $\Phi_0 = h/e$ (h is Planck's constant, e is the charge on the electron), confirmed that the QD supports coherent transport. As the experiment was set up with a two-terminal configuration, however, current conservation and time reversal symmetry lead[5] to $G(B) = G(-B)$ with B the magnetic field, restricting the phase of the AB oscillations to be either 0 or π. This means that only abrupt jumps between the two allowed phase values are possible[6,7]. Physically, this is a direct result of interference between the multiple paths that traverse the ring, obscuring the phase evolution of the transmission coefficient of the QD[7–10]. This phase rigidity does not exist in a double-slit-like interference experiment with a four-terminal configuration[5,11]. We used such a

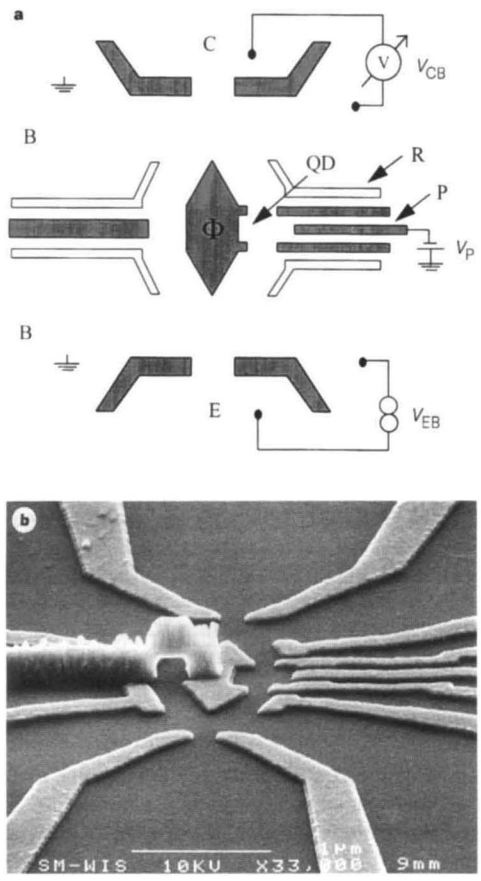

Figure 1 a, Schematic description of the double-slit interference experiment with a QD replacing one slit. The system is composed of three different regions, an emitter E, a collector C, and a base region B on both sides of the two slits. A contact to each region allows a four-terminal measurement. Reflector gates (R) are drawn in white. The excitation voltage V_{EB} is applied between emitter and base. The collector voltage V_{CB} is measured between base and collector. A voltage V_P on the plunger gate P changes the occupation of the QD. **b**, A top-view scanning electron micrograph of the device. The grey areas are metallic gates deposited on the surface of the heterostructure. The negatively biased gates define emitter and collector QPCs, a slit and a QD. A special lithographic technique, involving a metallic air bridge, is used to contact the central gate (which depletes the area between the two slits). The QD has an area $0.4 \times 0.4\,\mu m^2$ with both of its QPCs and the plunger gate (P) individually controlled. Reflector gates are added to increase the measured signal.

configuration to measure directly the magnitude and the phase of the transmission coefficient through a QD in the Coulomb blockade (CB) regime.

The actual double-slit interferometer consists of a patterned, high-mobility, two-dimensional electron gas, electron density $n_s = 3.0 \times 10^{11}\,cm^{-2}$, mobility $\mu = 1.6 \times 10^6\,cm^2\,V^{-1}\,s^{-1}$ at temperature $T = 4.2K$) formed 60 nm below the surface of a GaAs–AlGaAs heterostructure, with an elastic mean free path $l = 15\,\mu m$. The potential barriers are defined by negatively biased metal gates deposited on the surface of the heterostructure. Our four-terminal configuration (see Fig. 1a) consists of emitter E and collector C constrictions, called quantum point contacts (QPC), and a base region B in between. The base contacts serve as draining reservoirs with a chemical potential $\mu_B = 0$. The E and C constrictions are separated by a barrier with two openings (slits); one slit consists of the QD whose behaviour we want to measure, and the other is a reference slit in a form of another QPC. The number of electrons in the QD is around $N_{el} \approx 200$, with an average energy spacing between discrete states $\Delta E \approx E_F/N_{el} = 55\,\mu eV$, where E_F is the Fermi energy. Collector and emitter QPCs support only one transverse mode, thus producing a planar electronic wave front in the far field. As the collector signal is too small to be measured in an entirely open configuration, we incorporate additional barriers which reflect the emitted diverging electrons into the two slits and subsequently towards the collector (the white gates in Fig. 1a, called R). All measurements are done in a dilution refrigerator ($T_{lattice} = 15\,mK$, $T_{el} \approx 80\,mK$) with an a.c. excitation voltage $V_{EB} = 10\,\mu V$ applied across the emitter QPC.

At low temperatures both the phase coherence length and the elastic mean free path of the electrons exceed the entire sample size. Using the multiprobe conductance formula[5], we can see that the current at the collector QPC, I_C, is given by $I_C = (2e^2/h)(\tau_{EC}V_{EB} \pm \tau_C V_{CB})$, where V_{EB} is the injection voltage, and τ_{EC} and τ_C are the transmission probabilities from emitter to collector and through the collector QPC respectively. The open-circuit collector voltage ($I_C = 0$), $V_{CB} = (V_{EB}/\tau_C)\tau_{EC}$, leads directly to the transmission probability τ_{EC}, which in turn is a coherent sum over all path amplitudes from E to C. For the double slit case $t_{EC} = t_{QD} + t_{sl}$, where $|t_{EC}|^2 = \tau_{EC}$, t_{QD} is the transmission amplitude associated with the path traversing the QD, and t_{sl} refers to the reference path passing through the QPC slit on the left. A magnetic flux, Φ, threading the area, A, enclosed by these two classical paths results in an AB phase difference $\Delta\varphi = 2\pi\Phi/\Phi_0$ between the two interfering paths. For single-channel transmission:

$$\tau_{EC} = |t_{QD} + e^{i\Delta\varphi} \cdot t_{sl}|^2 \quad (1)$$

Assuming fully coherent transport through the QD, the interference term is proportional to $|t_{sl}||t_{QD}|\cos[\Delta\varphi + \theta(t_{sl}) - \theta(t_{QD})]$, where $\theta(t_{sl})$ and $\theta(t_{QD})$ account for the phase accumulated in the two corresponding paths. The transmission probability τ_{EC} is therefore expected to oscillate as a function of magnetic field with a period corresponding to the addition of one flux quantum to the area enclosed by the paths. As the phase accumulated in the reference path is to a good approximation constant, a change in the phase of t_{QD} leads to a similar change in the phase of the oscillating collector signal.

One must make sure that the added reflectors (R) are not preventing backscattered electrons from being collected by the base contacts; otherwise multiple path interference might occur, and higher-periodicity AB oscillations and phase rigidity might dominate[7]. We checked this by opening the QD, leaving only one of its QPCs functional, so that this served as an adjustable barrier adding to the accumulated phase in this path. As hoped, we found a smooth phase shift in the oscillating collector voltage with no higher harmonics (with periods Φ_0/n) as this QPC was adjusted. These results strongly suggest that the two direct paths predominantly contribute to the interference.

The QD is defined by adjusting the resistance of its QPCs to be greater than $h/2e^2$, so that it is in the CB regime with well separated energy levels, namely $\Gamma < \Delta E$, where Γ is the resonance width. Moreover, because we adjust the openings so that $k_B T < \Gamma$ ($k_B T \approx 7\,\mu eV$), the width of the conductance peak is determined by Γ and not by the temperature. Scanning the plunger gate voltage, V_P, we find pronounced resonances in V_{CB}, as expected for a QD in the CB regime (Fig. 2a), on top of a large background that results from the reference path. The asymmetry of the resonance peaks is a result of interference with the reference path. When a magnetic field is applied and the QD is being tuned to conduct, the collector signal shows AB oscillations with the expected period $\Delta B = \Phi_0/A = 3.5\,mT$. This confirms the results of Yacoby *et al.*[3] that transport through the QD is coherent. Figure 2b shows examples of AB oscillations measured at four specified points on the Coulomb peak seen in Fig. 2a. A smooth phase shift of the AB oscillations, on the scale of the resonance width, is observed. This phase shift gives

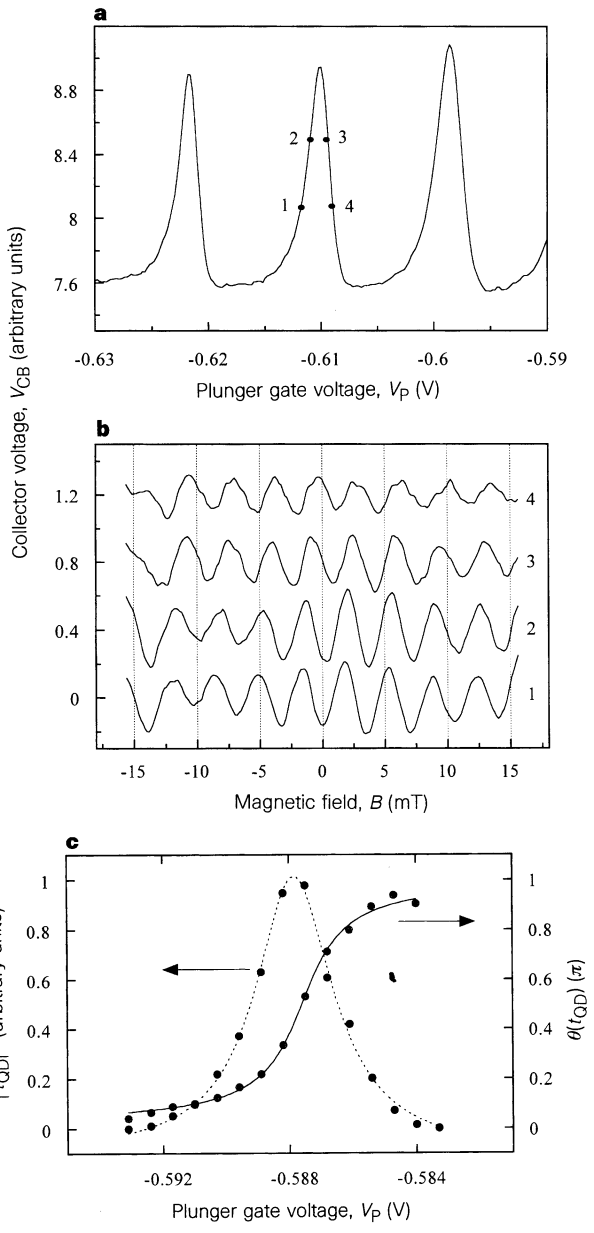

Figure 2 a, Resonance peaks as a function of the plunger gate voltage. **b**, A series of interference patterns taken at specified positions on a peak in **a**. The traces are shifted vertically for clarity. **c**, Bare resonance peak $|t_{QD}|^2$, obtained from the magnitude of the AB oscillations, and absolute value of the accumulated phase $\theta(t_{QD})$. The expected phase behaviour in a Breit-Wigner model (solid line) and a lorentzian fit to the resonance peak (dotted line) are shown.

directly the phase shift of the transmission coefficient of the QD. For a complete picture we record the AB interference oscillations at many points along a resonance peak and do a complex Fourier transform of the data. The phase evolution along one peak, seen in Fig. 2c, shows a monotonic rise by almost π near the maximum of the resonance.

We model the QD as a double barrier system confining a well with quasi-bound states. The transmission amplitude through such a system shows resonances near the energies of the quasi-bound states, E_n, described by the Breit–Wigner formula[12]

$$t_{QD} = C_n \cdot \frac{i\Gamma/2}{E - E_n + i\Gamma/2} \qquad (2)$$

where E is the energy of the incident carriers, Γ is the width of the resonant level, and C_n is a complex prefactor. Both depend on the coupling between the resonant states and the leads connecting the dot to the reservoirs. The phase of the transmission coefficient, given by

$$\theta(t_{QD}) = \theta_n + \arctan\frac{2}{\Gamma}(E - E_n) \qquad (3)$$

changes by π from one side of the resonance to the other (θ_n is the phase of C_n). To find the qualitative behaviour of $|t_{QD}|$ we measure the magnitude of the AB oscillations, which is proportional to $|t_{QD}|$ (see equation (1)). As can be seen in Fig. 2c, both magnitude and phase agree well with the prediction of equation (3). These results clearly show that the phase evolution of the transmission coefficient within a resonance peak is correctly described by a Breit–Wigner behaviour.

We now discuss measurements that probe the phase of the transmission coefficient for different CB peaks. Figure 3c shows the phase for a series of five successive peaks seen in Fig. 3a. We find a very similar phase behaviour for all resonances, as suggested by Yacoby *et al.*[3]. As the plunger gate voltage increases, the QPCs of the QD open slightly because of an electrostatic influence, and coupling to the reservoirs increases. Therefore, the Coulomb peaks widen and overlap, thus reducing the overall phase variation. These results demonstrate unambiguously that successive resonances of a QD have the same phase behaviour.

Another striking feature of the results is the sharp drop of the phase, by π, in the tail of each peak on a scale much smaller than Γ or k_BT. We stress that even though this sharp phase change resembles the one observed in a two-terminal measurement that forces rigidity of the phase, its physical origin is different, directly associated with the QD. Figure 3b shows the amplitude of the AB oscillations, which are proportional to $|t_{QD}|$, as a function of the plunger gate voltage. We see that the phase jump occurs when the oscillation amplitude vanishes, namely when $t_{QD} = 0$. The fact that $|t_{QD}|$ vanishes although the conductance of the complete system is not at a minimum (Fig. 3a) is a direct result of interference with the reference arm.

We now briefly discuss the phase behaviour of consecutive resonances. In a simple one-dimensional resonant tunnelling model, one expects the phase of the transmission coefficient to differ by π for each successive resonance. This was not observed in our experiment. For resonant tunnelling through an arbitrary system, the phase of the prefactor in equation (2), $\theta(C_m) = \theta_n$, depends on the overlap between the wavefunctions of the quasi-bound states in the QD and those in the leads, and thus in general is expected to be different for successive resonant states. Because at zero magnetic field time-reversal symmetry holds, the wavefunctions of the quasi-bound states in the QD can be chosen to be real, leading to a phase θ_n with only two possible values[9,13]: $\theta_n = \theta_0 \pm \pi/2$. When considering the case of a circular[9] or a rectangular[10] QD, the phase difference of consecutive resonances, $\Delta\theta = \theta_n - \theta_{n+1}$, depends on the symmetry of the QD; successive resonances both in phase ($\Delta\theta = 0$) and out of phase ($\Delta\theta = \pi$) are possible. In our system we do not expect a particular symmetry and thus such single-particle arguments cannot explain why large sequences of resonances (up to 10 peaks) have the same phase. Another approach, taken by Levy Yeyati *et al.*[8], uses the Friedel sum rule for the case of a QD embedded in one arm of an AB ring. Our results indicate that this model, which predicts a phase shift of π for every added charge e in the whole system (AB ring and QD), is not applicable in the present case.

The appearance of a second energy scale in the phase jump between resonances also cannot be understood as well in a non-interacting picture. Because we find experimentally that each peak has a similar phase behaviour, we model the QD as a sum of displaced Breit–Wigner amplitudes each with the same phase. We find that a phase rise of π within a peak is followed by a phase drop

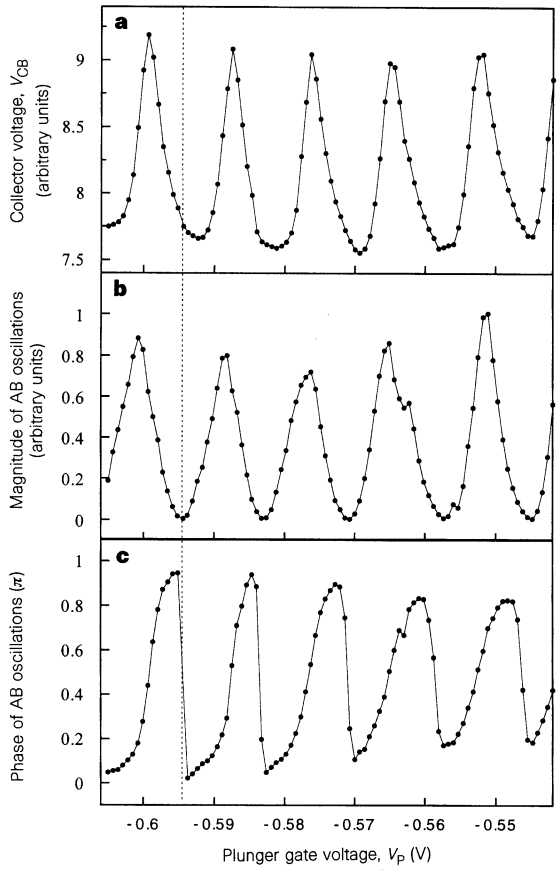

Figure 3 a, A series of resonance peaks as a function of plunger gate voltage; **b**, the magnitude of the AB oscillations; and **c**, the corresponding phase all obtained from the interference patterns taken at the marked points. The connecting lines serve only as a guide to the eye. The phase has a periodic behaviour which repeats itself at each resonance. Note the sharp phase jump between resonances.

of π, but the fact that this is on the same energy scale is in clear contradiction to our experimental results. In a recent interference experiment[13] we measured the phase of the reflection coefficient of a QD. In this experiment, again, the phase behaviour within a resonance could be well described by a single-particle model, but away from the resonance, near the points of minimum conductance, the behaviour, as in this case, is not well understood. □

Received 4 July; accepted 10 December 1996.

1. Van Houten, H., Beenakker, C. W. J. & Staring, A. A. W. in *Single Charge Tunnelling–Coulomb Blockade Phenomena in Nanostructures* (eds Grabert, H. & Devoret, M. H.), (Plenum, New York, 1992).
2. Meirav, U. & Foxman, E. B. *Semicond. Sci. Technol.* **10,** 255–284 (1995).
3. Yacoby, A., Heiblum, M., Mahalu, D. & Shtrikman, H. *Phys. Rev. Lett.* **74,** 4047–4050 (1995).
4. Aronov, A. G. & Sharvin, Yu. V. *Rev. Mod. Phys.* **59,** 755–779 (1987).
5. Büttiker, M. *Phys. Rev. Lett.* **57,** 1761–1764 (1986).
6. Gefen, Y., Imry, Y. & Azbel, M. Ya. *Phys. Rev. Lett.* **52,** 129–132 (1984).
7. Yacoby, A., Schuster, R. & Heiblum, M. *Phys. Rev.* B**53,** 9583–9586 (1996).
8. Levy Yeyati, A. & Büttiker, M. *Phys. Rev.* B**52,** 14360–14363 (1995).
9. Hackenbroich, G. & Weidenmüller, H. A. *Phys. Rev. Lett.* **76,** 110–113 (1996).
10. Bruder, C., Fazio, R. & Schoeller, H. *Phys. Rev. Lett.* **76,** 114–117 (1996).
11. Yacoby, A., Heiblum, M., Umansky, V., Shtrikman, H. & Mahalu, D. *Phys. Rev. Lett.* **73,** 3149–3152 (1994).
12. Breit, G. & Wigner, E. *Phys. Rev.* **49,** 519–531 (1936).
13. Buks, E. *Phys. Rev. Lett.* **77,** 4664–4667 (1996).

Acknowledgements. We thank Y. Gefen, Y. Levinson, Y. Oreg, N. Questembert, M. Schechter, F. von Oppen and H. A. Weidenmüller for discussions. This work was partly supported by a MINERVA grant, a MINERVA fellowship (R.S.) and a grant from the Israeli National Academy.

Correspondence should be addressed to R.S. (e-mail: rschuster@vnet.ibm.com).

Bacterial templating of ordered macrostructures in silica and silica–surfactant mesophases

Sean A. Davis*, Sandra L. Burkett*, Neil H. Mendelson† & Stephen Mann*

* *School of Chemistry, University of Bath, Bath BA2 7AY, UK*
† *Department of Molecular and Cellular Biology, University of Arizona, Tucson, Arizona 85721, USA*

The synthesis of inorganic frameworks with specified and organized pore networks is of potential importance in catalysis[1,2], separation technology[3] and biomaterials engineering[4,5]. Ordered arrangements of porous channels have been produced in silica-based materials by post-synthetic removal of surfactant templates from inorganic–organic mesostructures[6,7]. The resulting pore sizes are commensurate with the packing dimensions of the organic molecules, and are currently limited to length scales of up to 10 nm. Here we show how a bacterial superstructure, consisting of a thread of coaligned multicellular filaments of *Bacillus subtilis*[8,9], can be used to extend the length scale of inorganic materials patterning. We produce ordered macroporous fibres of either amorphous silica or ordered mesoporous silica[6,7] (MCM-41) by template-directed mineralization of the interfilament spaces followed by removal of organic material by heating to 600 °C. The inorganic macrostructures consist of a macroporous framework of 0.5-μm-wide channels with curved walls of either silica or mesoporous silica, 50 to 200 nm in thickness. The formation of ordered pores in the MCM-41 replica on both the mesoscopic and macroscopic length scales illustrates how supramolecular and supercellular templates might be combined for the fabrication of inorganic materials with structural hierarchy.

Our approach to using a bacterial superstructure to extend the length scale of materials templating in silica-based systems is illustrated in Fig. 1. Individual multicellular filaments of *B. subtilis* are coaligned by slowly drawing a macroscopic thread from a web culture[8,9]. The superstructure of the bacterial thread resembles the arrangement of hexagonal packing of surfactant cylinders in the surfactant–water H_1 phase[10], except that there is an increase in length scale of two orders of magnitude. In both cases, the interstitial spaces and contact edges represent a continuum for patterned inorganic mineralization. But whereas the 1-nm-wide contact spaces of the surfactant arrays can be readily bridged through the condensation of silicate anions associated with the surfactant headgroups in the synthesis of MCM-41[10], the formation of a coherent wall structure in the much larger void volume of the bacterial superstructure requires extensive *in situ* polymerization. Thus, we use silica-based nanoparticles, rather than molecular species, as the primary building block of mineralization within the 100- to 200-nm wide interfilament spaces.

Previous studies have shown that inorganic minerals can be precipitated on and within *B. subtilis* thread by drawing fibres from web cultures enriched in soluble metal (Ca^{2+}, Fe(II/III), Cu(II)) salts and drying in air[11,12]. To infiltrate the preformed bacterial superstructure with inorganic nanoparticles, we exploited the observation that dried unmineralized bacterial thread swells in water to 1.4 and 1.2 times the original length and width, respectively, without loss of structural integrity[13]. In addition, the swollen hydrated thread contracts to its original dimension when dried in air. We use this reversible swelling property to consolidate the infiltrated nanoparticles so that interconnecting mineral walls are formed within the interfilament spaces (Fig. 1). For example, drying of threads dipped into a silica sol gives rigid white fibres with a